Inorganica Chimica Acta 368 (2011) 74–83

Contents lists available at ScienceDirect

Inorganica Chimica Acta

journal homepage: www.elsevier.com/locate/ica

Diamidato-bis(diphenylphosphino) platinum(II) complexes: Synthesis, characterization, and reactivity in the presence of acid

Rebecca A. Swanson [b], Ryan S. Haywood [a], Joseph B. Gibbons [b], Kyle E. Cordova [a], Brian O. Patrick [c], Curtis Moore [d], Arnold L. Rheingold [d], Christopher J.A. Daley [a,*]

[a] Department of Chemistry and Biochemistry, University of San Diego, San Diego, CA 92110, USA
[b] Department of Chemistry, Western Washington University, Bellingham, WA 98225-9150, USA
[c] Department of Chemistry, University of British Columbia, Vancouver, BC, Canada V6T 1Z3
[d] Department of Chemistry and Biochemistry, University of California, San Diego, La Jolla, CA 92093, USA

ARTICLE INFO

Article history:
Received 12 August 2010
Received in revised form 16 December 2010
Accepted 20 December 2010
Available online 28 December 2010

Keywords:
Platinum–amidato complexes
Bis(phosphino) ligands
Trost ligand
X-ray crystal structures
NMR characterization
Protonation study

ABSTRACT

The reaction of $Pt(COD)Cl_2$, where COD is 1,5-cyclooctadiene, with one equivalent of a diamidato-bis(phosphino) Trost ligand ((*R*,*R*)-**2** = *N*,*N*′-bis(2-diphenylphosphino-1-benzoyl)-(1*R*,2*R*)-1,2-diaminocyclohexane, (*R*,*R*)-**3** = *N*,*N*′-bis(2-diphenylphosphino-1-naphthoyl)-(1*R*,2*R*)-1,2-diaminocyclohexane, or (±)-**4** = *N*,*N*′-bis(2-diphenylphosphino-1-benzoyl)-1,2-bis(aminobenzene)) in the presence of base afforded square planar diamidato-bis(phosphino) platinum(II) complexes (*R*,*R*)-**2**-Pt, (*R*,*R*)-**3**-Pt, (±)-**4**-Pt. Characterization of all complexes included the solution and solid state structure determination of each complex based on multinuclear NMR and X-ray analyses, respectively. Stability of the complexes in acid was examined on addition of HCl to (*R*,*R*)-**2**-Pt in chloroform and compared to the unreactive nature of the similar diamidato-bis(phosphino) complex **1**-Pt (**1** = 1,2-bis-*N*-[2′-(diphenylphosphino)benzoyl]diaminobenzene) in the presence of acid. Protonation of the bound amidato nitrogen atoms of (*R*,*R*)-**2**-Pt was observed along with decoordination of the nitrogen atoms from the platinum(II) center producing (*R*,*R*)-**2**-$PtCl_2$ in quantitative yield by NMR analysis. Confirmation of the product was made on comparison of the NMR spectra to that of authentic (*R*,*R*)-**2**-$PtCl_2$ prepared on reaction of $Pt(COD)Cl_2$ with (*R*,*R*)-**2** in CH_2Cl_2 and characterized by single-crystal X-ray diffraction analysis and NMR spectroscopy. Results add to the knowledge of rich coordination chemistry of bis(phosphino) ligands with late transition metals, metal–amidato chemistry, and has implications in catalysis.

1. Introduction

Our group is interested in ligands that contain amide-N atom(s) with the potential to participate in metal binding. Broad interest in these ligand systems stems from the intriguing properties [1] that metal-amidato complexes boast in areas such as catalyst development [2], medicinal chemistry [3], and bioinorganic chemistry [4–6]. In nature, metal–amidato coordination complexes play significant roles in the oxidized form of the P-Cluster of nitrogenase [4], the A-Cluster of CODH/acetyl Co-A synthase [5], and the mononuclear Fe- or Co-containing active site of nitrile hydratase [6]. Based on such findings, continued investigation into the coordination chemistry and reactivity of metal amidato systems remains of considerable interest. We have investigated the chemistry of the Trost designed diamidato-bis(phosphino) series of ligands (Fig. 1: Ligands **2**, **3**, and **4**), which has been widely used in palladium catalyzed asymmetric allylic alkylations [7]. Our interest stemmed from the structural similarities of Trost–metal complexes, with the Trost ligand bound in a tetracoordinate diamidato-bis(phosphino) fashion, to the backbone structure of the distal nickel center in CODH/acetyl Co-A synthase; containing two carboxamido nitrogen atoms and two phosphine units which are substitutes for the two native thiolate groups found in the enzyme [5]. Interest in these ligands is broadened since bis(phosphino) ligands have received much attention over the last several decades owing in major part to their use in coordination chemistry [8] and enantioselective catalysis [9]. Of note, both palladium- [7,10] and platinum-phosphino [11] complexes have been shown to be highly successful catalysts for numerous organic transformation reactions. We [12] and others [13] reported on the coordination versatility of the Trost ligand in palladium(II) complexes, being capable of binding either in a bidentate bis(phosphino) fashion or a tetradentate diamidato-bis(phosphino) fashion (Fig. 1: Complex **B**, e.g. (*R*,*R*)-**2**-Pd). The latter species is significant in Trost–palladium catalyzed allylic alkylation reactions as it shuts down the catalytic cycle as a catalytically inactive species. In comparison to its palladium chemistry, the platinum chemistry of the Trost ligands is less well known with

* Corresponding author. Tel.: +1 619 260 4033; fax: +1 619 260 2211.
E-mail address: cjdaley@sandiego.edu (C.J.A. Daley).

0020-1693/$ - see front matter © 2010 Elsevier B.V. All rights reserved.
doi:10.1016/j.ica.2010.12.056

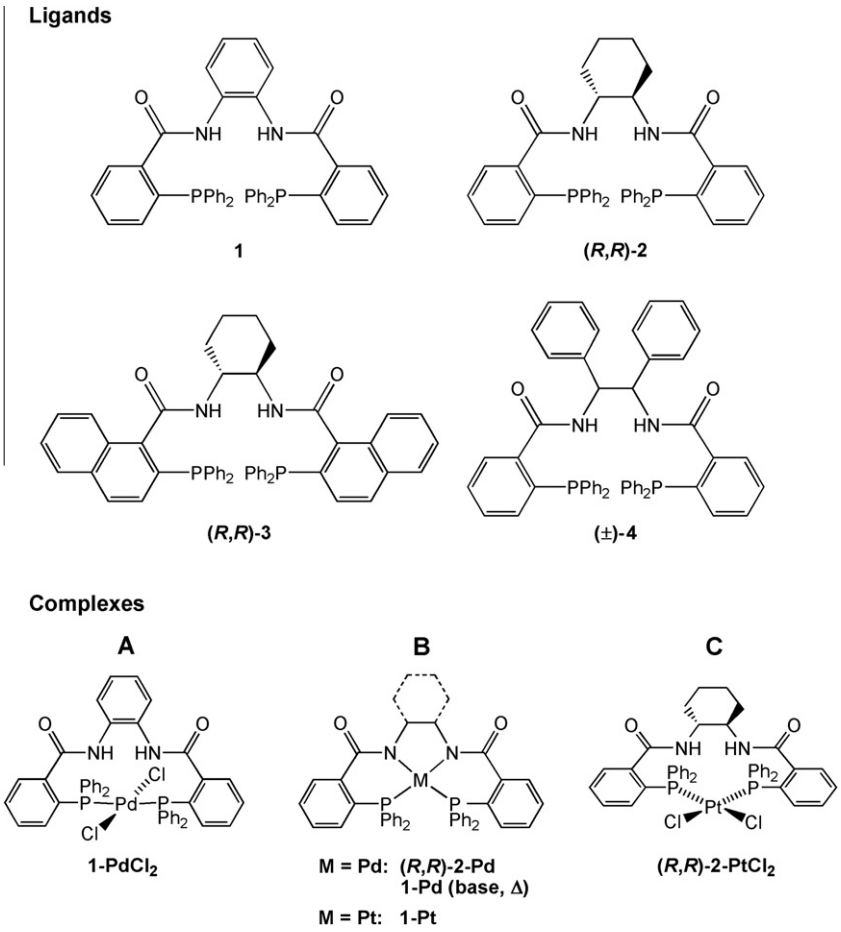

Fig. 1. Structures of the Süss-Fink (**1**) and Trost ligands ((*R*,*R*)-**2**, (*R*,*R*)-**3**, and (±)-**4**) (top) and their reported Pd and Pt complexes (bottom).

only one crystallographic report on (*R*,*R*)-**2** coordinating not in its tetradentate form but rather its bidentate bis(phosphino) form at room temperature with platinum(II) as (*R*,*R*)-**2**-$PtCl_2$ (Fig. 1: Complex **C**) [14].

More recently, it was reported that the coordination chemistry of Trost ligand on palladium(II) complexes contrasts that of the versatile ligand 1,2-bis-*N*-[2′-(diphenylphosphino)benzoyl]diaminobenzene (Fig. 1: Ligand **1**), an asymmetric analog of the Trost ligand, developed by Süss-Fink and co-workers [15]. Ligand **1** is reported to form **1**-$PdCl_2$ (Fig. 1: Complex **A**), where **1** coordinates solely in its bidentate form as a *trans*-spanning ligand with palladium(II) at room temperature even in the presence of excess base, which is unlike the Trost complexes [15a]. It was later determined that with heat in the presence of K_2CO_3, the amide protons can be deprotonated and the tetradentate diamidato-bis(phosphino) palladium(II) complex **1**-Pd forms (Fig. 1: Complex **B**) [15b]. However, in contrast to its palladium chemistry, **1** is reported to form solely the tetracoordinate diamidato-bis(phosphino) platinum(II) complex **1**-Pt (Fig. 1: Complex **B**) even in the presence of excess acid as noted by an unchanging $^{31}P\{^1H\}$ NMR when HCl was added [15a]. The latter complex again contrasts that reported for the Trost ligand set where (*R*,*R*)-**2**-$PtCl_2$ (Fig. 1: Complex **C**) is observed under similar reaction conditions used to prepare **1**-Pt.

The versatile and controllable coordination of ligands such as the Süss-Fink ligand **1**, favoring one coordination mode depending on the metal center (Pd versus Pt) and temperature used, is of further interest in catalysis where the catalytic activity of a species is dependent on the coordination mode of the ligand. As example, **1**-Pd (Fig. 1: Complex B) has been reported as the probable catalytically active species for palladium catalyzed Suzuki-Mayaura cross-coupling reactions [15b] while the analogous Trost complex (*R*,*R*)-**2**-Pd is catalytically inactive in allylic alkylation reactions with its bidentate bis(phosphino) ligation mode, without metal-amidato bonding, being the active species [16]. As such, synthesizing and investigating coordination complexes of Trost and related ligands has broad appeal. Thus, based on the interesting and versatile coordination properties of **1**, and on the limited platinum chemistry of the Trost ligand set, we set out to prepare and investigate a series of platinum(II) Trost complexes to further understand the nature of these intriguing systems. Herein we report on the coordination versatility of (*R*,*R*)-**2**, (*R*,*R*)-**3**, and (±)-**4** through the direct synthesis and characterization, in both solution and solid states, of three tetracoordinate Trost-based diamidato-bis(phosphino) platinum(II) complexes. Furthermore, we report on the stability and reactivity of the Trost diamidato-bis(phosphino) platinum(II) complex in the presence of acid and compare it to that of **1**-Pt.

2. Experimental

2.1. General

All chemicals were ACS reagent grade or better and used without further purification unless otherwise stated. Solvents methylene chloride, diethyl ether, acetonitrile and THF were obtained from an Innovative Technology solvent purification system and were de-oxygenated prior to use. All reactions were carried out under a dry nitrogen or argon atmosphere, unless specified otherwise. All NMR data was obtained on either a Varian Mercury

(300 MHz) or an Inova (500 MHz) NMR spectrometer. ^{1}H and $^{13}C\{^{1}H\}$ NMR chemical shifts are referenced to tetramethylsilane (TMS) at 0.00 ppm. $^{31}P\{^{1}H\}$ NMR chemical shifts are referenced to 85% H_3PO_4 at 0.0 ppm.

2.2. Syntheses

2.2.1. Synthesis of (*R*,*R*)-**2**-Pt

To a 25 mL flask were added (*R*,*R*)-**2** (0.150 g, 0.217 mmol) and Pt(COD)Cl_2 (0.0815 g, 0.218 mmol) dissolved in THF (10 mL). NaH (0.0203 g, 0.508 mmol, 60% in oil) was weighed into a 50 mL side arm flask and THF (10 mL) was added. The solution containing the ligand and Pt(COD)Cl_2 was transferred via cannula to the flask containing the NaH. The yellow solution was heated at 50 °C. The solution continued to stir for 24 h. After this time a white solid had precipitated out of solution. The solution was inverse filtered to yield (*R*,*R*)-**2**-Pt (0.068 g, 0.077 mmol) in 35% yield. X-ray crystals were obtained by dissolving (*R*,*R*)-**2**-Pt in CH_2Cl_2 and performing a diethyl ether vapor diffusion. ^{1}H NMR ($CDCl_3$, 500 MHz) δ 8.47 (dd, 2H), 7.48 (t, 2H), 7.35 (m, 4H), 7. 26 (dd, 4H), 7.18 (m, 6H), 7.13 (m, 4H), 7.08 (m, 4H), 6.67 (dd, 2H), 3.69 (m, 2H), 2.65 (br d, 2H), 1.61 (m, 2H), 1.54 (br q, 2H), 1.31 (br t, 2H). $^{13}C\{^{1}H\}$ NMR ($CDCl_3$, 126 MHz) δ 167.7 (m), 144.8 (m), 133.6 (m), 133.5 (m), 131.9 (m), 131.6 (s), 131.3 (m), 131.1 (s), 130.8 (s), 129.4 (m), 128.8 (m), 128.7 (m), 128.4 (m), 125.6 (m), 125.1 (m), 68.0 (s), 31.5 (s), 26.4 (s). $^{31}P\{^{1}H\}$ NMR ($CDCl_3$, 202 MHz) δ 5.4 ($^{1}J_{P-Pt}$ = 3150 Hz).

2.2.2. Synthesis of (*R*,*R*)-**3**-Pt

In a glove box, (*R*,*R*)-**3** (0.299 g, 0.378 mmol) and NaOMe (0.085 g, 1.57 mmol) were dissolved in THF (6 mL) in a 20 mL sample vial. In a separate vial, Pt(COD)Cl_2 (0.141 g, 0.377 mmol) was dissolved in THF (5 mL). The solutions were stirred for 10 min then the mixture of (*R*,*R*)-**3** and NaOMe was added to the platinum complex solution. The resulting solution was stirred for 2 h. The solution was transferred to a 50 mL sidearm flask, removed from the glove box, and placed on a Schlenk line. The stirred solution was refluxed for 14 h. No significant precipitate was noted after this time. The solvent was removed under vacuum and the residue was re-dissolved in minimal methylene chloride, filtered through a Celite plug, and the solvent was again removed under vacuum. The resulting crude product was loaded onto a Biotage Isolera automated column system and purified by running 12 column volumes in a 1:1 ethyl acetate:hexanes and then changing gradient to 2:1 ethyl acetate:hexanes. The pure product (*R*,*R*)-**3**-Pt was isolated in 5.3% yield (0.0198 g, 0.0201 mmol). ^{1}H NMR ($CDCl_3$): δ = 8.45 (br d, 2H), 7.75 (m, 4H), 7.63 (br d, 2H), 7.44–7.48 (m, 6H), 7.29 (m, 2H), 7.24 (m, 4H), 7.20 (m, 2H), 6.89 (br s, 8H), 6.37 (br t, 2H), 3.70 (m, 2H), 3.36 (br d, 2H), 1.70 (m, 2H), 1.48 (br t, 2H), 1.22 (m, 2H). $^{13}C\{^{1}H\}$ NMR ($CDCl_3$, 126 MHz) δ 176.7 (m), 146.8 (m), 135.9 (t), 135.2 (s), 133.4 (t), 131.9 (s), 131.1 (m), 130.7 (s), 128.7 (t), 128.5 (t), 128.3 (m), 128.1 (s), 128.0 (s), 127.9 (s), 127.5 (s), 125.9 (m), 68.7 (s), 31.4 (s), 26.2 (s). $^{31}P\{^{1}H\}$ NMR ($CDCl_3$, 202 MHz) δ 2.1 ($^{1}J_{P-Pt}$ = 3130 Hz).

2.2.3. Synthesis of (±)-**4**-Pt

To a 100 mL flask were added (±)-**4** (0.1503 g, 0.1896 mmol) and Pt(COD)Cl_2 (0.0715 g, 0.191 mmol) dissolved in THF (7 mL). NaH (0.0167 g, 0.418 mmol, 60% in oil) was weighed into a 100 mL side arm flask and THF (10 mL) was added. The solution containing the ligand and Pt(COD)Cl_2 was transferred via cannula to the flask containing the NaH. The yellow solution was heated at 50 °C. After one hour of heating the solid had gone into solution. The solution continued to stir for ~17 h. After this time a brown-pink solid precipitated. The solution was inverse filtered to yield (±)-**4**-Pt (0.062 g, 0.063 mmol) in 33% yield. X-ray crystals were obtained by dissolving (±)-**4**-Pt in CH_2Cl_2 and performing a diethyl ether vapor diffusion. ^{1}H NMR ($CDCl_3$, 500 MHz) δ 8.65 (dd, 2H, e), 7.68 (dd, 4H), 7.45 (m, 8H), 7.32 (t, 4H), 7.15 (m, 10H), 6.79 (t, 4H), 6.68 (dd, 4H), 6.49 (d, 2H), 6.38 (dd, 2H). $^{13}C\{^{1}H\}$ NMR ($CDCl_3$, 126 MHz) δ 165.2 (m), 143.0 (s), 142.2 (m), 136.2 (m), 133.0 (m), 132.3 (m), 131.9 (s), 131.5 (m), 131.4 (s), 130.1 (s), 128.7 (m), 128.4 (m), 127.8 (s), 127.5 (m), 127.2 (s), 127.0 (m), 126.7 (m), 126.2 (m), 125.7 (s), 66.0 (s). $^{31}P\{^{1}H\}$ NMR ($CDCl_3$, 202 MHz) δ 4.1 ($^{1}J_{P-Pt}$ = 3120 Hz).

2.3. Reaction of (*R*,*R*)-**2**-Pt with HCl

In an NMR tube, 22 mg of (*R*,*R*)-**2**-Pt was dissolved in $CDCl_3$ (previously de-oxygenated). Both ^{1}H and $^{31}P\{^{1}H\}$ NMR analyses was performed on the sample to ensure it was pure then excess HCl was bubbled through the solution for 1 min. The HCl was prepared via the reaction of conc. H_2SO_4 with NaCl in a test tube equipped with a N_2 inlet stream to push the HCl formed through to a dry ice/acetone trap and finally to a needle that was immersed in the NMR sample. After the addition, the NMR tube was shaken by hand for 2 min and then ^{1}H and $^{31}P\{^{1}H\}$ NMR spectra were recorded immediately. The NMR corresponded to those for (*R*,*R*)-**2**-$PtCl_2$ reported below.

2.4. Isolation of (*R*,*R*)-**2**-$PtCl_2$

To a 10 mL round bottom flask was added Pt(COD)Cl_2 (5.2 mg, 1.4×10^{-5} mol) and (*R*,*R*)-**2** (9.6 mg, 1.4×10^{-5} mol) and $CHCl_3$ (5 mL). The solution was stirred under N_2 for 16 h then solvent was removed under vacuum. The residue was dissolved in minimal CH_2Cl_2 and crystallized via vapor diffusion of Et_2O into the solution. A single crystal of (*R*,*R*)-**2**-$PtCl_2$ was analyzed by X-ray diffraction and the crystal was then analyzed by ^{1}H and $^{31}P\{^{1}H\}$ NMR. The remaining unused solid (8.1 mg, 8.5×10^{-6} mol, 61%) was also analyzed by ^{1}H NMR and was shown to be the same as the crystal. ^{1}H NMR ($CDCl_3$, 500 MHz) δ 7.97 (m, 4H), 7.78 (d, 1H), 7.40 (m, 11H), 7.22 (m, 5H), 7.08 (m, 2H), 7.01 (dd, 1H), 6.94 (m, 1H), 6.85 (m, 3H), 4.53 (m, 1H), 3.22 (m, 1H), 2.72 (br d, 1H), 2.60 (br q, 1H), 1.93 (br d, 1H), 1.86 (br d, 1H), 1.64 (m, 1H), 1.46 (m, 1H), 1.31 (m, 1H), 0.82 (br q, 1H). $^{31}P\{^{1}H\}$ NMR ($CDCl_3$, 202 MHz) δ 11.1 ($^{1}J_{P-Pt}$ = 3880 Hz, 1P), 7.2 ($^{1}J_{P-Pt}$ = 3680 Hz, 1P).

2.5. X-ray crystallography

The crystal data for (*R*,*R*)-**2**-Pt, (*R*,*R*)-**3**-Pt, (±)-**4**-Pt, and (*R*,*R*)-**2**-$PtCl_2$ are collected in Table 1. Crystals of (*R*,*R*)-**2**-Pt, (*R*,*R*)-**3**-Pt, (±)-**4**-Pt, and (*R*,*R*)-**2**-$PtCl_2$ suitable for X-ray structure determination were obtained by vapor diffusion of diethyl ether into a concentrated solution of the compound of interest in CH_2Cl_2. Data were collected on a Bruker X8 APEX ((*R*,*R*)-**2**-Pt and (±)-**4**-Pt) or a Bruker Apex II ((*R*,*R*)-**3**-Pt and (*R*,*R*)-**2**-$PtCl_2$) diffractometer with graphite monochromated Mo Kα radiation at 173 K or 100 K (Table 1). The data were integrated using the Bruker SAINT ((*R*,*R*)-**2**-Pt and (±)-**4**-Pt) [17] or SHELXTL ((*R*,*R*)-**3**-Pt and (*R*,*R*)-**2**-$PtCl_2$) [18] software programs and the structures were solved by direct methods [19]. All refinements were performed using the SHELXTL [20] crystallographic software package of Bruker-AXS. Neutral atom scattering factors were taken from Cromer and Waber [21]. Anomalous dispersion effects were included in Fcalc [22]; the values for $\Delta f'$ and $\Delta f''$ were those of Creagh and McAuley [23]. The values for the mass attenuation coefficients are those of Creagh and Hubbell [24]. Further details specific to each analysis are given below.

2.5.1. (*R*,*R*)-**2**-Pt

A colorless prism crystal of $C_{44}H_{38}N_2O_2P_2Pt$ having approximate dimensions of 0.12 × 0.12 × 0.25 mm was mounted on a glass

Table 1
Selected crystallographic data for (*R*,*R*)-**2**-Pt, (*R*,*R*)-**3**-Pt, **(±)-4**-Pt, and (*R*,*R*)-**2**-$PtCl_2$.[a]

Parameter	(*R*,*R*)-**2**-Pt	(*R*,*R*)-**3**-Pt	(±)-**4**-Pt	(*R*,*R*)-**2**-$PtCl_2$
Formula	$C_{44}H_{38}N_2O_2P_2Pt$	$C_{52}H_{42}N_2O_2P_2Pt{\cdot}CH_2Cl_2$	$C_{52}H_{40}N_2O_2P_2Pt{\cdot}CH_2Cl_2$	$C_{44}H_{40}Cl_2N_2O_2P_2Pt{\cdot}2CH_2Cl_2$
Formula weight (g/mol)	883.79	1068.83	1066.82	1128.58
a (Å)	9.7335 (3)	11.8905 (15)	11.0681 (2)	10.7943 (3)
b (Å)	17.4583 (6)	13.2544 (17)	19.7119 (4)	19.8851 (5)
c (Å)	21.0741 (7)	28.515 (4)	20.6359 (4)	21.8166 (5)
α (°)	90.0	90.00	90.0	90.0
β (°)	90.0	90.00	95.901 (1)	90.0
γ (°)	90.0	90.00	90.0	90.0
V (Å^3)	3581.1 (2)	4494.0 (10)	4478.4 (2)	4682.8 (2)
Z	4	4	4	4
Space group	$P2_12_12_1$ (#19)	$P2_12_12_1$ (#19)	$P2_1/n$ (#14)	$P2_12_12_1$ (#19)
Crystal system	orthorhombic	orthorhombic	monoclinic	orthorhombic
D_{calc} (g/cm^3)	1.639	1.580	1.582	1.601
T (K)	173.1 (1)	100 (2)	173.1 (1)	100
μ (Mo K) (mm^{-1})	4.05	3.357	3.37	3.45
Total reflections	47153	20619	44736	18421
2θ Range (°)	1.5–27.9	1.69–25.36	2.86–52.76	1.9–28.2
Unique reflections	8536	7767	10711	9920
Parameters	460	559	559	549
Flack χ	−0.021 (3)	0.004 (4)	–	−0.009 (5)
R_1[b], wR_2[c]	0.025, 0.044	0.0216, 0.0537	0.045, 0.069	0.045, 0.077

[a] See CCDC-783095, CCDC-783096, CCDC-783097, and CCDC-783098 structure files for more information.
[b] $R_1 = \Sigma||F_o| - |F_c||/\Sigma|F_o|$, $I \geq 2\sigma(I)$; $wR_2 = \{\Sigma[w(F_o^2 - F_c^2)^2]/\Sigma[w(F_o^2)^2]\}^{1/2}$, all data.
[c] $S = \{\Sigma[w\{(F_o^2 - F_c^2)^2\}]/(n-p)\}^{1/2}$.

fiber. The data were collected to a maximum 2θ value of 55.8° in a series of phi and omega scans in 0.50° oscillations with 5.0 s exposures. The crystal-to-detector distance was 38.94 mm. Of the 47153 reflections that were collected, 8536 were unique (R_{int} = 0.047; Friedels not merged); equivalent reflections were merged. Data were corrected for absorption effects using the multi-scan technique (SADABS [25]), with minimum and maximum transmission coefficients of 0.482 and 0.615, respectively. The data were corrected for Lorentz and polarization effects. All non-hydrogen atoms were refined anisotropically. All C–H hydrogen atoms were included in calculated positions but were not refined. This enantiomer was chosen on the basis of the refined Flack parameter [26]. The maximum and minimum peaks on the final difference Fourier map corresponded to 0.52 and −0.41 e Å^{-3}, respectively.

2.5.2. (*R*,*R*)-**3**-Pt·CH_2Cl_2

A yellow block 0.35 × 0.37 × 0.38 mm^3 in size was mounted on a Cryoloop with Paratone-N oil. Data were collected in a series of phi and omega scans using in 0.50° oscillations with 10 s exposures and was 99.4% complete to 25.00° in θ. The crystal-to-detector distance was 60 mm. Of the 20619 reflections that were collected, 7767 were unique (R_{int} = 0.0324). The data were scaled using the SADABS [27] software program. The material crystallizes with one molecule of methylene chloride in the asymmetric unit. All non-hydrogen atoms were refined anisotropically by full-matrix least-squares on F^2 (SHELXL-97) [28]. All hydrogen atoms were constrained relative to their parent atom using the appropriate HFIX command in SHELXL-97. The compound was determined to be chiral with atoms C12 and C17 being both *R*-configuration with a Flack [29] parameter of 0.035(5). The maximum and minimum peaks on the final difference Fourier map corresponded to 1.003 and −0.793 e Å^{-3}, respectively.

2.5.3. (±)-**4**-Pt·CH_2Cl_2

A colorless prism crystal of $C_{52}H_{40}N_2O_2P_2Pt{\cdot}CH_2Cl_2$ having approximate dimensions of 0.15 × 0.15 × 0.25 mm was mounted on a glass fiber. Data were collected in a series of phi and omega scans in 0.50° oscillations with 10.0 s exposures to a maximum 2θ value of 55.8°. The crystal-to-detector distance was 38.94 mm. Of the 44736 reflections that were collected, 10711 were unique (R_{int} = 0.053); equivalent reflections were merged. Data were corrected for absorption effects using the multi-scan technique (SADABS [21]), with minimum and maximum transmission coefficients of 0.448 and 0.603, respectively. The data were corrected for Lorentz and polarization effects. The material crystallizes with one molecule of methylene chloride in the asymmetric unit. All non-hydrogen atoms were refined anisotropically. All C–H hydrogen atoms were included in calculated positions but were not refined. The maximum and minimum peaks on the final difference Fourier map corresponded to 1.05 and −1.04 e Å^{-3}, respectively.

2.5.4. (*R*,*R*)-**2**-$PtCl_2{\cdot}2CH_2Cl_2$

A colorless rod crystal of $C_{44}H_{42}Cl_2N_2O_2P_2Pt{\cdot}2CH_2Cl_2$ having approximate dimensions of 0.27 × 0.18 × 0.09 mm^3 was mounted on a glass fiber. Data were collected in a series of phi and omega scans using in 0.50° oscillations with 10 s exposures and was 99.2% complete to 25.00° in θ. The crystal-to-detector distance was 60 mm. Of the 18421 reflections that were collected, 9920 reflections were unique (R_{int} = 0.0287). The data were scaled using the SADABS [27] software program. The material crystallizes with two molecules of methylene chloride in the asymmetric unit. All non-hydrogen atoms were refined anisotropically by full-matrix least-squares on F^2 (SHELXL-97) [28]. All hydrogen atoms were constrained relative to their parent atom using the appropriate HFIX command in SHELXL-97. The compound was determined to be chiral with atoms C8 and C13 being both *R*-configuration with a Flack parameter of −0.009(5). The final cycle of full-matrix least-squares refinement on F^2 was based on 9920 reflections, 6 restraints, and 549 variable parameters and converged with unweighted and weighted agreement factors of: $R_1 = \Sigma||F_o| - |F_c||/\Sigma|F_o| = 0.0360$; $wR_2 = [\Sigma(w(F_o^2 - F_c^2)^2)/\Sigma w(F_o^2)^2]^{1/2} = 0.0734$. The maximum and minimum peaks on the final difference Fourier map corresponded to 1.227 and −1.058 e Å^{-3}, respectively.

3. Results and discussion

3.1. Synthesis of diamidato-bis(phosphino) platinum complexes

Earlier studies revealed the divergent behavior of the Trost ligand (*R*,*R*)-**2** from that of **1** in their palladium(II) complexes

where **1** does not form tetradentate **1**-Pd in solution at room temperature even in the presence of added base [15a]. Rather, **1**-$PdCl_2$ is formed where **1** is coordinated solely through its phosphorus atoms in a *trans*-ligating fashion (Fig. 1). Complex **1**-Pd is formed in high yield only on reaction of **1** and $Pd(OAc)_2$ in the presence of two equivalent of base and heat [15b]. In contrast, we have shown that the Trost ligands begin to form the corresponding **L**-Pd (**L** = (*R*,*R*)-**2**, (*R*,*R*)-**3**, or (±)-**4**) complexes at room temperature in the presence of added base and are isolated in high yields on heating (16 h, 50 °C, >85% yields) [12]. Further coordination differences are noted in the platinum chemistry of these ligand systems where reaction of **1** with $Pt(COD)Cl_2$ in CH_2Cl_2 produces the tetracoordinate **1**-Pt complex [15a], while reaction of (*R*,*R*)-**2** with $Pt(COD)Cl_2$ under similar conditions is reported to only form the bidentate bis(phosphano)platinum(II) complex (*R*,*R*)-**2**-$PtCl_2$ (Scheme 1) even in the presence of excess acid [14]. Based on our palladium work, the Trost ligands deprotonate and appear to form tetradentate complexes more readily than **1**. With this knowledge, we set out to prepare the Trost-based analogs of **1**-Pt ((*R*,*R*)-**2**-Pt, (*R*,*R*)-**3**-Pt, and (±)-**4**-Pt). The desired complex (*R*,*R*)-**2**-Pt was prepared by a direct route with molar equivalents of (*R*,*R*)-**2** reacting with $Pt(COD)Cl_2$ in the presence of base (2.2 equivalent NaH) in THF at 50 °C overnight, conditions that produced the analogous palladium complexes in high yields. The product (*R*,*R*)-**2**-Pt precipitated from solution and was collected by filtration in a 35% yield. Using similar conditions, (*R*,*R*)-**3**-Pt and (±)-**4**-Pt were prepared. Complex (*R*,*R*)-**3**-Pt precipitated from solution and was collected by filtration in 33% yield. Unlike the other complexes, (±)-**4**-Pt did not precipitate from solution and was only obtained in pure form after column chromatography of the evaporated product residue in 5% yield. We note that addition of base and heat were necessary to prepare the complexes (*R*,*R*)-**2**-Pt, (*R*,*R*)-**3**-Pt, and (±)-**4**-Pt. To confirm their structure, (*R*,*R*)-**2**-Pt, (*R*,*R*)-**3**-Pt, and (±)-**4**-Pt were characterized both in the solution and solid states by NMR and X-ray crystallographic methods, respectively.

3.2. Solution structure

Complex (*R*,*R*)-**2**-Pt was characterized in $CDCl_3$. Amidato coordination was evident from the lack of an amide proton signal in the ^1H NMR (Fig. 2: top) as well as the presence of a signature peak at 8.47 ppm (H_f), which was a key indicator of amidato coordination in the palladium(II) analogs [12]. The ^1H NMR shows only 14 unique proton environments indicating that (*R*,*R*)-**2**-Pt behaves as a C_2-symmetric system in solution. Coordination of the phosphines and corroboration of the C_2-symmetric nature of the complex is confirmed by $^{31}P\{^1H\}$ NMR where only one signal is observed at 5.4 ppm (s) with Pt-satellites signals (d, $^1J_{P-Pt}$ = 3150 Hz) at 33% intensity relative to the central peak owing to the coupling to ^{135}Pt (S = ½). The $^1J_{P-Pt}$ coupling constant is consistent with a *cis*-coordinated bis(phosphino) platinum(II) complexes, as $^1J_{P-Pt}$ of *cis*-coordination in platinum(II) complexes is reported to typically be greater than 3000 Hz, while $^1J_{P-Pt}$ of the *trans*-configuration is smaller than 3000 Hz [29]. The ^1H NMR signals were assigned (Fig. 2) from NMR analyses including HMQC, HMBC, COSY, NOESY, and ROESY as well as from comparisons to the assignments of their palladium(II) analog complexes [12]. A brief overview of some of the main features is given below. For (*R*,*R*)-**2**-Pt, protons H_a (3.68 ppm) were identified based both on the chemical shift and HSQC and the downfield signal for H_f protons (8.47 ppm) was identified from analysis of the HMBC spectrum of (*R*,*R*)-**2**-Pt as it coupled to the carbonyl carbon atom (167.6 ppm). The protons on the pendant phenyl groups of the phosphines were assigned based on COSY and $^1H\{^{31}P\}$ analyses but it is noted that the assignment of the $H_{o,m,p}$ and $H_{o',m',p'}$ ring spin systems was arbitrary and may be reversed.

Similarly to (*R*,*R*)-**2**-Pt, complexes (*R*,*R*)-**3**-Pt and (±)-**4**-Pt were characterized in solution by NMR analysis; both display C_2-symmetry in solution based on the number and integration of the ^1H NMR signals (Fig. 2) as well as the single $^{31}P\{^1H\}$ NMR signals observed for each complex ((*R*,*R*)-**3**-Pt, 2.1 ppm, $^1J_{P-Pt}$ = 3130 Hz; (±)-**4**-Pt, 4.1 ppm, $^1J_{P-Pt}$ = 3120 Hz). Furthermore, each complex had the characteristic downfield ^1H signal at ~8.5 ppm signaling tetradentate coordination as noted earlier. For (*R*,*R*)-**3**-Pt, the assignment of the naphthyl ring backbone proton signal for H_1 was confirmed by ROESY analysis, where the signal was shown to correlate to the cyclohexyl backbone proton H_c (3.36 ppm). On examining the structure, the only aromatic proton that is in proximity to an aliphatic proton is that of H_1, this is further supported by the lack of ROE or NOE cross peaks observed between the cyclohexyl protons of (*R*,*R*)-**2**-Pt and any of its backbone aromatic protons owing to the greater distance between the protons in that complex. In (±)-**4**-Pt the downfield signal for H_f (8.65 ppm) was confirmed by

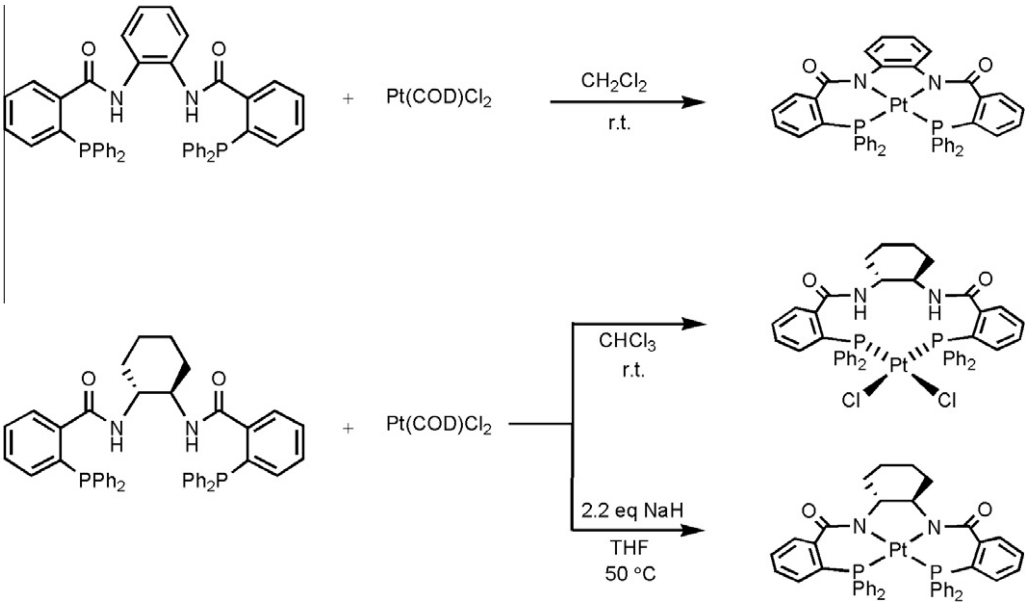

Scheme 1. Reaction scenarios observed on reacting Süss-Fink (**1**: top) and Trost ((*R*,*R*)-**2**: bottom) ligands with $Pt(COD)Cl_2$.

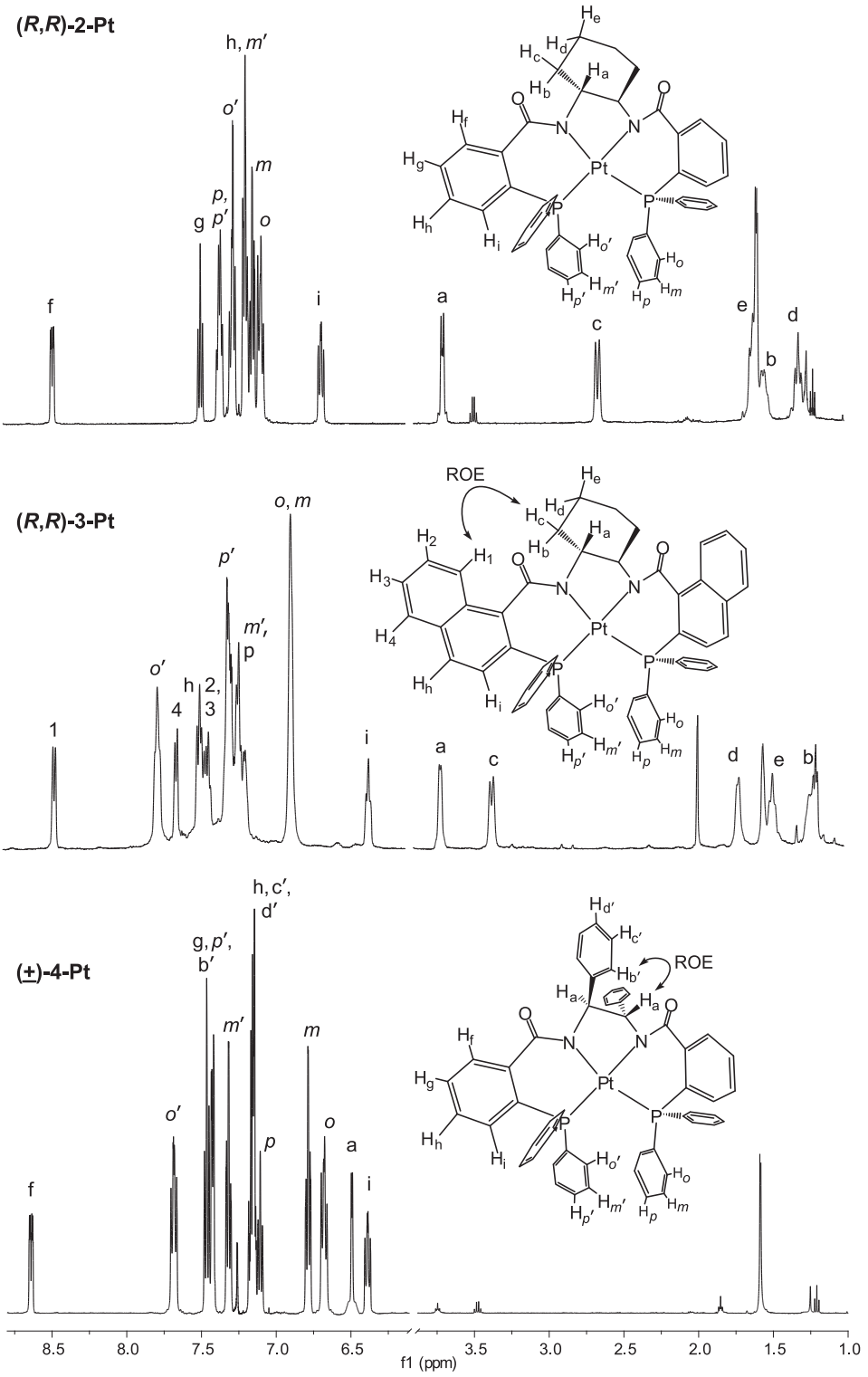

Fig. 2. ^{1}H NMR spectra of complexes (*R*,*R*)-**2**-Pt, (*R*,*R*)-**3**-Pt, and (±)-**4**-Pt (top to bottom, respectively) in $CDCl_3$.

the coupling to the carbonyl carbon signal (165.2 ppm) in the HMBC spectrum analogous to the analysis of (*R*,*R*)-**2**-Pt. Assignments of the backbone substituent phenyl ring protons ($H_{b'}$–$H_{d'}$) were made based on the ROE cross peak observed between H_a (6.49 ppm) and the overlapping signals at 7.45 ppm. The latter peak contains the signal for $H_{b'}$, the *ortho*-protons, as they are the only protons of a phenyl group that are in close proximity to H_a. As was the case with (*R*,*R*)-**2**-Pt, the assignments of the $H_{o,m,p}$ and $H_{o',m',p'}$ ring spin systems was arbitrary and may be reversed in both (*R*,*R*)-**3**-Pt and (±)-**4**-Pt.

In solution, NMR analysis indicates that each complex contains a C_2-symmetric diamidato-bis(phosphino) square planar geometry. Analysis of the X-ray diffraction data of each complex was performed in order to determine the solid state structures.

3.3. Solid state structure

The products were characterized in the solid state by X-ray crystallography using crystals obtained via diethyl ether vapor diffusion into a concentrated solution of (*R*,*R*)-**2**-Pt, (*R*,*R*)-**3**-Pt, or (±)-**4**-Pt in CH_2Cl_2 (Tables 1 and 2; Fig. 3). Complexes (*R*,*R*)-**3**-Pt and (±)-**4**-Pt co-crystallize with one molecule of methylene chloride but there is no meaningful interaction between the two molecules in either case. The complexes are all square planar about the platinum as confirmed by the summation of the bond angles between the coordinating atoms (P1–Pt–N1 + N1–Pt–N2 + N2–Pt–P2 + P2–Pt–P1 = 360° ideally for square planar; (*R*,*R*)-**2**-Pt = 360.0°; (*R*,*R*)-**3**-Pt = 359.6°; (±)-**4**-Pt = 360.1°). Expressed in another manner, the atoms Pt1, P1, P2, N1 and N2 are found to be almost coplanar, with an average deviation of ~0.006 Å ((*R*,*R*)-**2**-Pt), ~0.006 Å ((*R*,*R*)-**3**-Pt), ~0.057 Å ((±)-**4**-Pt) relative to the average plane set by the nitrogen and phosphorus atoms and the metal lies out of this plane by 0.009 Å ((*R*,*R*)-**2**-Pt), 0.096 Å ((*R*,*R*)-**3**-Pt), 0.029 Å ((±)-**4**-Pt). These are similar to the structure of **1**-Pt [15a] where the average deviation was found to be ~0.067 Å with the Pt metal outside the plane by 0.078 Å.

As was noted with the analogous Pd complexes, (±)-**4**-Pt maintains pseudo-C_2-symmetry in the solid state while the C_2-symmetry is broken in (*R*,*R*)-**2**-Pt and (*R*,*R*)-**3**-Pt as the cyclohexyl backbone is out of the square plane set by the phosphorus, nitrogen, and palladium atoms. The Pt–N1 and Pt–N2 bond lengths are equivalent (<3σ) within (*R*,*R*)-**2**-Pt and (±)-**4**-Pt as are the Pt–P1 and Pt–P2 bond lengths within (*R*,*R*)-**2**-Pt and (*R*,*R*)-**3**-Pt. In the cases of the Pt–N bond lengths of (*R*,*R*)-**3**-Pt (Pt–N: Δ ~0.02 Å) and the Pt–P bond lengths of (±)-**4**-Pt (Pt–P: Δ ~0.01 Å) they are only very slightly dissymmetric. Overall, the bond lengths in each complex are in the range of those reported for similar bis(phosphino)-platinum(II) complexes including **1**-Pt (Pt–P: 2.243(2) and 2.34(2) Å; Pt–N: 2.035(6) and 2.067(5) Å) [15a].

3.4. Stability of (*R*,*R*)-**2**-Pt in acid

Süss-Fink noted that **1**-Pt is unchanged in the presence of excess concentrated HCl based on $^{31}P\{^1H\}$ NMR analyses [15a]. Unlike **1**, the Trost ligand (*R*,*R*)-**2** was reported to form the bidentate bis(phosphino) platinum(II) complex (*R*,*R*)-**2**-$PtCl_2$ when directly reacted with $Pt(COD)Cl_2$ in $CHCl_3$ [14]. On slow evaporation of the latter reaction solution, crystals of (*R*,*R*)-**2**-$PtCl_2$ suitable for single crystal X-ray diffraction analysis were obtained and were used to confirm its identity. Here, we have reported the preparation of the tetracoordinate Trost–platinum(II) complexes (*R*,*R*)-**2**-Pt, (*R*,*R*)-**3**-Pt and (±)-**4**-Pt, indicating that the Trost ligand system may be more coordinationally versatile in nature than **1**. They appear to allow more flexibility in coordination mode dependent on the pH and temperature of the complex under investigation. To test the versatility, we compared the stability of (*R*,*R*)-**2**-Pt in the presence of acid to that of **1**-Pt, which is unchanged. Based on

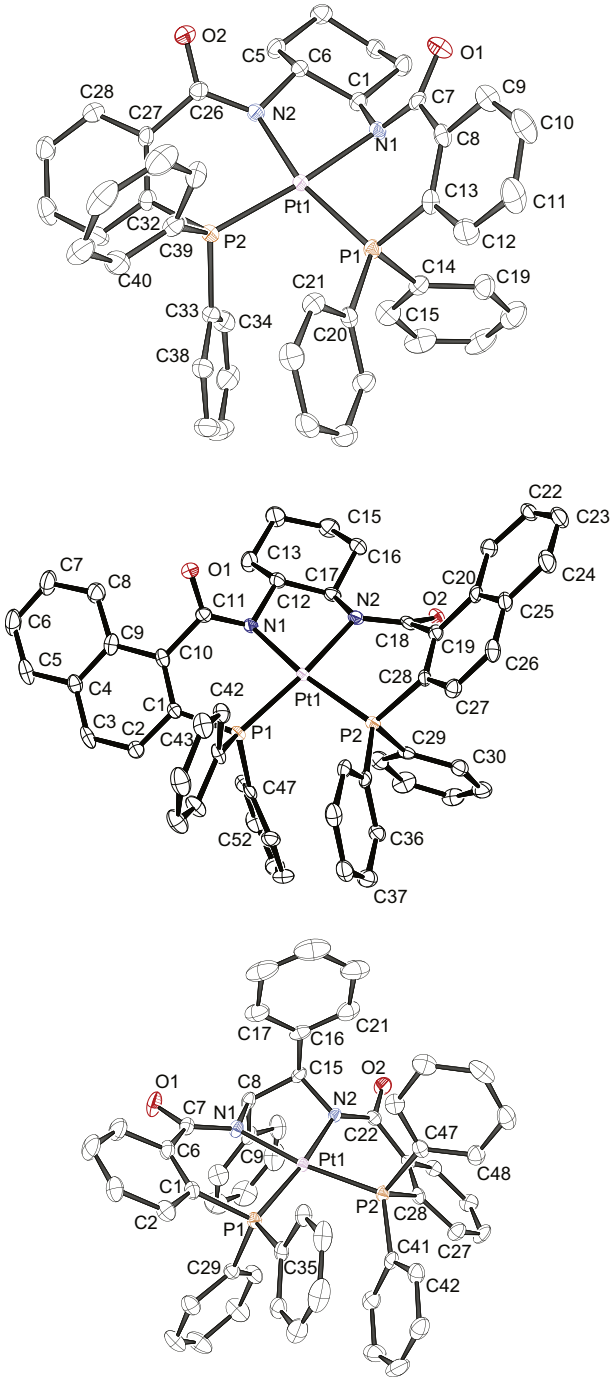

Fig. 3. X-ray crystallographic structures of (*R*,*R*)-**2**-Pt, (*R*,*R*)-**3**-Pt, and (±)-**4**-Pt (top to bottom, respectively). Ellipsoids are shown at 50% probability. Hydrogen atoms and solvates are not shown for clarity.

Table 2
Selected bond distances (Å) and angles (°) for Complexes (*R*,*R*)-**2**-Pt, (*R*,*R*)-**3**-Pt, (±)-**4**-Pt, and (*R*,*R*)-**2**-$PtCl_2$.

(*R*,*R*)-**2-Pt**		(*R*,*R*)-**3-Pt**		(±)-**4-Pt**		(*R*,*R*)-**2-PtCl$_2$**	
Pt–N1	2.065(2)	Pt–N1	2.070(3)	Pt–N1	2.056(3)	Pt–Cl1	2.3752(10)
Pt–N2	2.064(2)	Pt–N2	2.091(3)	Pt–N2	2.051(3)	Pt–Cl2	2.3859(14)
Pt–P1	2.2362(8)	Pt–P1	2.2361(10)	Pt–P1	2.2283(8)	Pt–P1	2.2735(15)
Pt–P2	2.2349(7)	Pt–P2	2.2362(10)	Pt–P2	2.2363(9)	Pt–P2	2.2772(11)
N1–Pt–N2	82.41(9)	N1–Pt–N2	81.99(12)	N1–Pt–N2	82.81(11)	Cl1–Pt–Cl2	84.90(5)
N1–Pt–P1	84.07(7)	N1–Pt–P1	90.20(9)	N1–Pt–P1	89.13(8)	Cl1–Pt–P1	89.92(4)
N1–Pt–P2	173.96(6)	N1–Pt–P2	169.95(9)	N1–Pt–P2	170.73(8)	Cl1–Pt–P2	171.14(4)
N2–Pt–P1	166.47(7)	N2–Pt–P1	170.69(9)	N2–Pt–P1	170.64(8)	Cl2–Pt–P1	168.27(5)
N2–Pt–P2	91.61(7)	N2–Pt–P2	88.95(9)	N2–Pt–P2	88.12(8)	Cl2–Pt–P2	86.30(5)
P1–Pt–P2	101.91(3)	P1–Pt–P2	98.42(4)	P1–Pt–P2	100.07(3)	P1–Pt–P2	98.92(5)

the reported isolation of (*R*,*R*)-**2**-$PtCl_2$ [14], it was anticipated that (*R*,*R*)-**2**-$PtCl_2$ would be formed on addition of HCl to (*R*,*R*)-**2**-Pt.

As the X-ray structure report of (*R*,*R*)-**2**-$PtCl_2$ did not contain any other characterization data [14], we prepared (*R*,*R*)-**2**-$PtCl_2$ so as to further characterize it for comparison purposes to the product(s) obtained on addition of HCl to (*R*,*R*)-**2**-Pt. It was made on reacting a 1:1 mole ratio of (*R*,*R*)-**2** and $Pt(COD)Cl_2$ in CH_2Cl_2 at room temperature. Both X-ray diffraction and NMR analyses were performed on the product crystals (*R*,*R*)-**2**-$PtCl_2$ obtained from a vapor diffusion of pentane into the product solution. X-ray analysis was required to confirm the compound was indeed (*R*,*R*)-**2**-$PtCl_2$ (Tables 1 and 2 and Fig. 4) and is reported here for completeness. Of note, the earlier reported structure [14] was found to be monoclinic ($P2_1/n$) and is a $CHCl_3$ trisolvate while the one reported herein is orthorhombic ($P2_12_12_1$) with a CH_2Cl_2 disolvate. Overall, the structures of the main complex (*R*,*R*)-**2**-$PtCl_2$ (ignoring the solvates) are similar in geometry with minor deviations noted in the metal-ligand bond distances (Pt–$P_{(average)}$: 2.2583(12) and 2.2754(13) Å; Pt–$Cl_{(average)}$: 2.3525(12) and 2.3806(12) Å for the earlier and new structures, respectively) and the P–Pt–P bond angles (101.15(4)° and 98.92(5)° for the earlier and new structures, respectively).

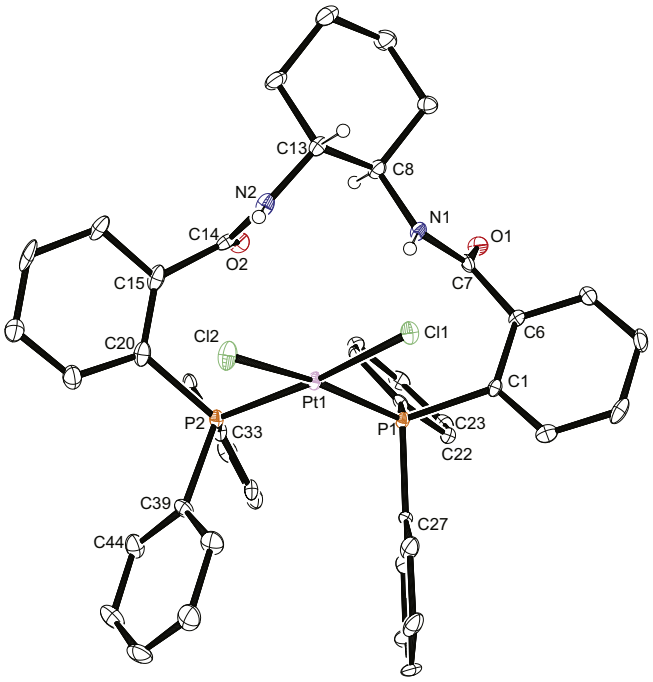

Fig. 4. X-ray crystallographic structure of (*R*,*R*)-**2**-$PtCl_2$. Ellipsoids are shown at 50% probability. Most hydrogen atoms and two co-solvated CH_2Cl_2 molecules are omitted for clarity.

With the NMR characterization of (*R*,*R*)-**2**-$PtCl_2$ obtained, the reactivity of (*R*,*R*)-**2**-Pt in the presence of acid was followed by ^1H and $^{31}P\{^1H\}$ NMR analyses. First, NMR spectra of (*R*,*R*)-**2**-Pt dissolved in $CDCl_3$ were taken, then excess HCl was bubbled through the solution and the mixture was re-analyzed by NMR to look for changes. On addition of the acid, there was an immediate change in both the ^1H and $^{31}P\{^1H\}$ NMR spectra. While the ^1H NMR spectrum was slightly complicated by the large ^1H signal for H_2O, the feature signal of (*R*,*R*)-**2**-Pt at 8.47 ppm disappeared, indicating likely decoordination of the carboxamido nitrogen atoms. The identification of the ^1H NMR signals for the protonated amide nitrogens N–*H* were not observed as expected owing to exchange with the excess H^+/H_2O in solution.

Unexpectedly, the loss of C_2-symmetry of the product was noted through the doubling of the number of proton signals as compared to (*R*,*R*)-**2**-Pt. The $^{31}P\{^1H\}$ NMR spectrum of the reaction mixture indicated only one phosphorus containing species was in solution. It had two broad signals at 11.1 ppm ($^1J_{P-Pt}$ = 3880 Hz) and 7.2 ppm ($^1J_{P-Pt}$ = 3680 Hz) with the expected Pt-coupling satellites that are indicative of *cis*-coordination of the phosphines. Comparison of the NMR spectra of the *in-situ* product of reaction between (*R*,*R*)-**2**-Pt and HCl with that of the (*R*,*R*)-**2**-$PtCl_2$ crystals (Fig. 5) showed them to be identical indicating protonation of (*R*,*R*)-**2**-Pt amidato nitrogens occurs in the presence of HCl (Scheme 2). We note, addition of excess base to the NMR sample along with heating does show the reformation of the deprotonated (*R*,*R*)-**2**-Pt

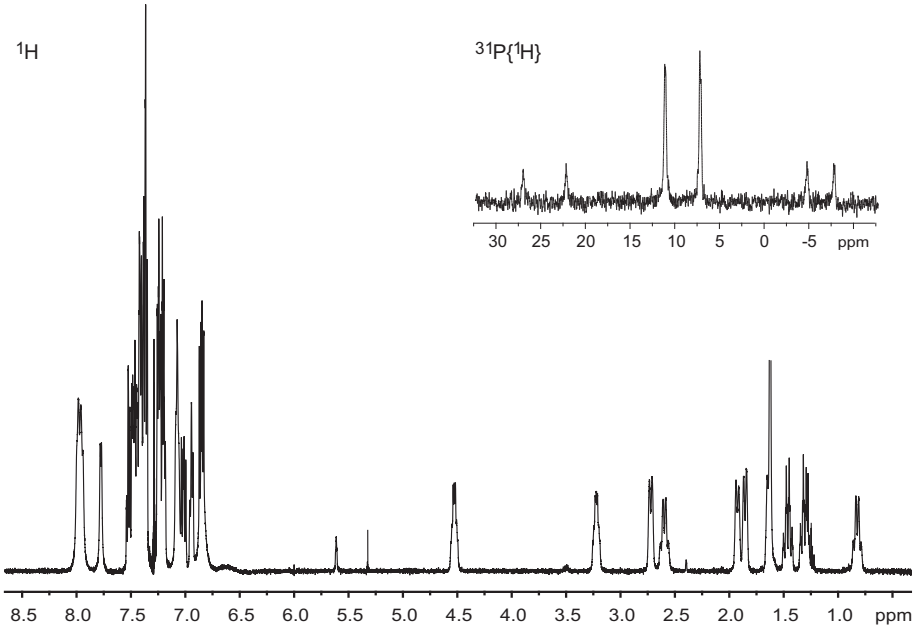

Fig. 5. ^1H NMR and $^{31}P\{^1H\}$ NMR (inset) spectra of (*R*,*R*)-**2**-$PtCl_2$, the reaction product formed *in-situ* on reaction of (*R*,*R*)-**2**-Pt with HCl in $CDCl_3$. Loss of C_2-symmetry is noted by the presence of ten cyclohexyl proton signals in the 0.5–4.6 ppm range.

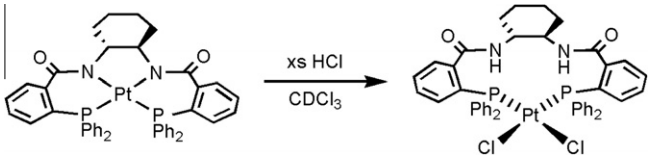

Scheme 2. Protonation reaction of (*R*,*R*)-**2**-Pt with HCl. Product (*R*,*R*)-**2**-$PtCl_2$ was identified on comparison to an authentic sample of (*R*,*R*)-**2**-$PtCl_2$.

complex as expected. While the crystal structures of (*R*,*R*)-**2**-$PtCl_2$ indicate the complex is not C_2-symmetric in the solid state, analogous to (*R*,*R*)-**2**-Pt and (*R*,*R*)-**3**-Pt, the dissymmetry is maintained in the solution state (Fig. 5) unlike in (*R*,*R*)-**2**-Pt and (*R*,*R*)-**3**-Pt. In both crystal structures of (*R*,*R*)-**2**-$PtCl_2$, intramolecular hydrogen bonds are observed between the N–H groups and the Cl atoms on the platinum. These interactions are likely maintained in solution and thus do not allow the fluxional processes necessary to make the complex C_2-symmetric in solution. In contrast, on formation of the tetracoordinate Trost–platinum(II) complexes (e.g. (*R*,*R*)-**2**-Pt), these hydrogen bonding interactions are removed, allowing the fluxional motion of the cyclohexyl rings to occur, making the complexes C_2-symmetric on the NMR timescale.

4. Conclusions

We have shown that the diamidato-bis(phosphino) Trost ligand systems have versatile coordination geometry with platinum(II) metal centers. Herein we have demonstrated that they can bind as tetradentate diamidato-bis(phosphino) ligands in their deprotonated form when heated in the presence of base through the synthesis and characterization of the three complexes (*R*,*R*)-**2**-Pt, (*R*,*R*)-**3**-Pt, and (±)-**4**-Pt. The ligands can also bind as neutral bidentate bis(phosphino) ligands (e.g. (*R*,*R*)-**2**-$PtCl_2$) as noted from an earlier report and our 1:1 reaction of (*R*,*R*)-**2** with Pt(COD)Cl_2 in the absence of base. Based on the acid reactivity studies with (*R*,*R*)-**2**-Pt, it was determined that (*R*,*R*)-**2**-Pt completely converts to (*R*,*R*)-**2**-$PtCl_2$ on addition of HCl. This is in stark contrast to the related Süss-Fink ligand **1**, which remains unchanged in the presence of excess HCl. That **1** is more selective in its binding makes it excellent for systems that require one specific coordination mode, assuming **1** adopts the desired mode. The Trost ligands are coordinatively flexible with the presence of acid or base biasing the binding mode from neutral bidentate bis(phosphino) coordination to dianionic tetradentate diamidato-bis(phosphino) coordination, respectively. This acid/base biasing may be useful in tuning the reaction systems involving Trost-metal complexes in order to ensure the appropriate bis(phosphino) or diamidato-bis(phosphino) complexes are maintained in solution. The importance of such coordination control is exemplified by the reports that the bidentate coordination complex is the active catalytic form [29] in palladium catalyzed allylic alkylation reactions while the tetradentate diamidato-bis(phosphino) coordination complex is reported to be the likely catalytically active species in **1**-Pd catalyzed Suzuki–Miyaura cross-coupling reactions [15a]. Based on this work, we are currently preparing to examine the effect of acid and base on a variety of potential palladium and platinum catalyzed reactions with the Trost ligand set.

Acknowledgments

K.E.C. thanks the McNair Foundation for funding. C.J.A.D. gratefully acknowledges the financial support of the National Science Foundation (RUI: CHE-0809266), Research Corporation (Cottrell College Science Award: CC#6100), and the University of San Diego and Western Washington University.

Appendix A. Supplementary material

CCDC 783095, 783096, 783097 and 783098 contain the supplementary crystallographic data for compounds (*R*,*R*)-**2**-Pt, (*R*,*R*)-**3**-Pt·CH_2Cl_2, (±)-**4**-Pt·CH_2Cl_2 and (*R*,*R*)-**2**-$PtCl_2$·$2CH_2Cl_2$), respectively. These data can be obtained free of charge from The Cambridge Crystallographic Data Centre via www.ccdc.cam.ac.uk/data_request/cif. Supplementary data associated with this article can be found, in the online version, at doi:10.1016/j.ica.2010.12.056.

References

[1] Examples of complexes and reactivity studies: (a) R.K. Thomson, F.E. Zahariev, Z. Zhang, B.O. Patrick, Y.A. Wang, L.L. Schafer, Inorg. Chem. 44 (2005) 8680;
(b) E. Hevia, J. Pérez, V. Riera, Organometallics 22 (2003) 257;
(c) B.-H. Huang, T.-L. Yu, Y.-L. Huang, B.-T. Ko, C.-C. Lin, Inorg. Chem. 41 (2002) 2987;
(d) V.Y. Kukushkin, A.J.L. Pombeiro, Chem. Rev. 102 (2002) 1771;
(e) H. Nagao, T. Hirano, N. Tsuboya, S. Shiota, M. Mukaida, T. Oi, M. Yamasaki, Inorg. Chem. 41 (2002) 6267;
(f) A.T. Vlahos, E.I. Tolis, C.P. Raptopoulou, A. Tsohos, M.P. Sigalas, A. Terzis, T.A. Kabanos, Inorg. Chem. 39 (2000) 2977.
[2] Selected catalyst examples: (a) T.E. Patten, C. Troeltzsch, M.M. Olmstead, Inorg. Chem. 44 (2005) 9197;
(b) P. Pelagatti, M. Carcelli, F. Calbiani, C. Cassi, L. Elviri, C. Pelizzi, U. Rizzotti, D. Rogolino, Organometallics 24 (2005) 5836;
(c) L.D. McPherson, M. Drees, S.I. Khan, T. Strassner, M.M. Abu-Omar, Inorg. Chem. 43 (2004) 4036;
(d) S. Battacharya, K. Snehalatha, V.P. Kumar, J. Org. Chem. 68 (2003) 2741;
(e) B.Y. Lee, X. Bu, G.C. Bazan, Organometallics 20 (2001) 5425;
(f) S. Nishino, M. Kunita, Y. Kani, S. Ohba, H. Matsushima, T. Tokii, Y. Nishida, Inorg. Chem. Commun. 3 (2000) 145;
(g) Y. Ishikawa, S. Ito, S. Nishino, S. Ohba, Y. Nishida, Z. Naturforsch. C: J. Biosci. 53 (1998) 378.
[3] (a) F.P. Intini, M. Lanfranchi, G. Natile, C. Pacifico, A. Tiripicchio, Inorg. Chem. 35 (1996) 1715;
(b) B. Higley, F.W. Smith, T. Smith, H.G. Gemmell, P.D. Gupta, D.V. Gvozdanovic, D. Graham, D. Hinge, J. Davidson, A. Lahiri, J. Nucl. Med. 34 (1993) 30;
(c) B.L. Zaret, J. Nucl. Med. 34 (1993) 1254;
(d) M.A. DeRosch, J.W. Brodack, G.D. Grummon, M.E. Marmion, D.L. Nosco, K.F. Deutsch, E. Deutsch, J. Nucl. Med. 33 (1992) 850.
[4] (a) S.M. Mayer, D.M. Lawson, C.A. Gormal, S.M. Roe, B.E. Smith, J. Mol. Biol. 292 (1999) 871;
(b) M.C. Jeannine, J. Christiansen, D.R. Dean, L.C. Seefeldt, Biochemistry 38 (1999) 5779.
[5] (a) G.H. Loew, D.L. Harris, Chem. Rev. 100 (2000) 407;
(b) C.G. Riordan, J. Biol. Inorg. Chem. 9 (2004) 509.
[6] (a) J.A. Kovacs, Chem. Rev. 104 (2004) 825;
(b) T.C. Harrop, P.K. Mascharak, Acc. Chem. Res. 37 (2003) 253;
(c) M. Odaka, M. Tsujimura, I. Endo, RIKEN 41 (2001) 58.
[7] (a) B.M. Trost, D.L. Van Vranken, C. Bingel, J. Am. Chem. Soc. 114 (1992) 9327;
(b) B.M. Trost, D.L. Van Vranken, Angew. Chem., Int. Ed. 31 (1992) 228.
[8] F.A. Cotton, G. Wilkinson, C.A. Murillo, M. Bochmann, Advanced Inorganic Chemistry, sixth ed., Wiley-Interscience, New York, 1999.
[9] (a) A. Börner (Ed.), Phosphorus Ligands in Asymmetric Catalysis, Synthesis and Applications, Wiley-VCH, Weinheim, Germany, 2008.;
(b) H.-U. Blaser, E. Schmidt (Eds.), Asymmetric Catalysis on Industrial Scale, Challenges, Approaches, and Solutions, Wiley-VCH, Weinheim, Germany, 2004.
[10] Selected examples: (a) D.S. Surry, S.L. Buchwald, Angew. Chem., Int. Ed. 47 (2008) 6338;
(b) R. Martin, S.L. Buchwald, Acc. Chem. Res. 41 (2008) 1461;
(c) C. Godard, B.K. Munoz, A. Ruiz, C. Claver, Dalton Trans. 7 (2008) 853;
(d) J.-C. Hierso, M. Beauperin, P. Meunier, Eur. J. Inorg. Chem. 24 (2007) 3767;
(e) K.H. Shaughnessy, Eur. J. Org. Chem. 8 (2006) 1827.
[11] Selected examples: (a) A. Sivaramakrishna, B.C.E. Makhubela, J.R. Moss, G.S. Smith, J. Organomet. Chem. 695 (2010) 1627;
(b) M.P. Shinde, X. Wang, E.J. Kang, H.-Y. Jang, Eur. J. Org. Chem. 35 (2009) 6091;
(c) T. Ohshima, Y. Miyamoto, J. Ipposhi, Y. Nakahara, M. Utsunomiya, K. Mashima, J. Am. Chem. Soc. 131 (2009) 14317;
(d) D. Brissy, M. Skander, P. Retailleau, G. Frison, A. Marinetti, Organometallics 28 (2009) 140;
(e) M. Colladon, A. Scarso, P. Sgarbossa, R.A. Michelin, G. Strukul, J. Am. Chem. Soc. 128 (2006) 14006;
(f) O. Fujimura, J. Am. Chem. Soc. 120 (1998) 10032.
[12] R.A. Swanson, B.O. Patrick, M.J. Ferguson, C.J.A. Daley, Inorg. Chim. Acta 360 (2007) 2455.
[13] K.R. Campos, M. Journet, S. Lee, E.J. Grabowski, R.D. Tillyer, J. Org. Chem. 70 (2005) 268.
[14] S. Burger, B. Therrien, G. Süss-Fink, Acta Crystallogr., Sect. E E60 (2004) m1163.
[15] (a) S. Burger, B. Therrien, G. Süss-Fink, Eur. J. Inorg. Chem. (2003) 3099;
(b) L. Chahen, L. Karmazin-Brelot, G. Süss-Fink, Inorg. Chem. Commun. 9 (2006) 1151.

[16] B.M. Trost, B. Breit, M.G. Organ, Tetrahedron Lett. 35 (1994) 5817.
[17] SAINT, Version 7.03A, Bruker AXS Inc., Madison, Wisconsin, USA, 1997–2003.
[18] G.M. Sheldrick, SHELXTL v. 5.10, Structure Determination Software Suite, Bruker AXS, Madison, Wisconsin, USA, 1998.
[19] SIR97, A. Altomare, M.C. Burla, M. Camalli, G.L. Cascarano, C. Giacovazzo, A. Guagliardi, A.G.G. Moliterni, G. Polidori, R. Spagna, J. Appl. Crystallogr. 32 (1999) 115.
[20] SHELXTL, Version 5.1, Bruker AXS Inc., Madision, Wisconsin, USA, 1997.
[21] D.T. Cromer, J.T. Waber, International Tables for X-ray Crystallography, vol. IV, The Kynoch Press, Birmingham, England, 1974 (Table 2.2 A).
[22] J.A. Ibers, W.C. Hamilton, Acta Crystallogr. 17 (1964) 781.
[23] D.C. Creagh, W.J. McAuley, in: A.J.C. Wilson (Ed.), International Tables for Crystallography, vol. C, Kluwer Academic Publishers, Boston, 1992, pp. 219–222 (Table 4.2.6.8).
[24] D.C. Creagh, J.H. Hubbell, in: A.J.C. Wilson (Ed.), International Tables for Crystallography, vol. C, Kluwer Academic Publishers, Boston, 1992, pp. 200–206 (Table 4.2.4.3).
[25] SADABS, Bruker Nonius Area Detector Scaling and Absorption Correction, vol. 2.10, Bruker AXS Inc., Madison, Wisconsin, USA, 2003.
[26] H.D. Flack, Acta Crystallogr., Sect. A 39 (1983) 876.
[27] Bruker, SADABS, Bruker AXS Inc., Madison, Wisconsin, USA, 2001.
[28] G.M. Sheldrick, Acta Crystallogr., Sect. A 64 (2008) 112.
[29] J.J. Macdougall, J.H. Nelson, F. Mathey, Inorg. Chem. 21 (1982) 2145.